

Gyroidal Metal–Organic Frameworks

Xiao-Ping Zhou, Mian Li, Jie Liu, and Dan Li*

Department of Chemistry, Shantou University, Guangdong 515063, P. R. China

 Supporting Information

ABSTRACT: The gyroid is ubiquitous for underlying the construction of natural substance and artificial zeolites, but it has been, surprisingly, overlooked by chemists who work in the field of metal–organic frameworks (MOFs). In this work, a series of gyroidal MOFs with *gie* topology, constructed from 1,2-bis((*SH*-imidazol-4-yl)methylene)hydrazine and octahedral metal ions, such as Zn^{II} , Mn^{II} , Cu^{II} , and Ni^{II} , have been synthesized. The Zn^{II} analogue, named as STU-1, shows exceptional thermal and chemical stabilities, and exhibits permanent porosity and CO_2 capture ability.

The gyroid (aka *G* surface),¹ as a supreme prototype that fills the gap between mathematics and physical sciences, is known to underlie various self-assembling structures ranging from inorganic and metal crystals to cell membranes and biopolymers,^{2,3} and most spectacularly, to butterfly wing scales.⁴ On the atomic and mesoscopic scales, this unique minimal surface has been found to direct the fabrication of several renowned inorganic zeolite-like materials, known as MCM-48,⁵ UCSB-7,⁶ SU-M,⁷ MSU-Ge-1,⁸ and ITQ-37.⁹ However, although ubiquitous in nature and artifact, the uniqueness and significance of the gyroid are yet to be identified in the flourishing field of metal–organic frameworks (MOFs),¹⁰ probably because of the lack of obvious attraction in terms of properties and certain design principles targeting gyroidal MOFs.

The crucial role of minimal surfaces in the construction of MOFs was demonstrated in an early work by Yaghi and co-workers,¹¹ who identified in MOF-14 the metal–organic building blocks can be assembled on a triply periodic *P* minimal surface. In comparison, the *G* minimal surface derives from, but is more complex than, the *P* and *D* minimal surface.^{1–3} It does not have any reflectional symmetry and contains no straight line, contradicting our common sense and visualization in the Euclidean space—perhaps this is the reason why the gyroid was discovered much later and is still overlooked by structural chemists who have been taking advantage of the tool of topology to understand the three-periodic nets in extended crystal structures.¹²

Here, we report a range of gyroidal MOFs, namely, STU-1 (Zn), 2 (Mn), 3 (Cu), and 4 (Ni), based on 1,2-bis((*SH*-imidazol-4-yl)methylene)hydrazine (BIm). They are a new branch of zeolitic imidazolate frameworks (ZIFs)^{13–16} with unprecedented topology (for MOFs) and in which the labyrinthine feature of the gyroid can be identified with crystalline ordering on the atomic scale. In most cases of ZIFs, the introduction of tetrahedral metal ions (e.g., Zn^{II} or Co^{II}) is a requisite to mimic the zeolitic topology based on the SiO_4 tetrahedron, while the flexible *M*–*Im*–*M*–*Im*–*M* (*M* = metal, *Im* = imidazolate) linkage gives rise to

the vast structural diversity of ZIFs.^{16,17} There are two main approaches to manipulate the conformation of this linkage: (i) by employing functionalized *Im* links to activate link–link interactions;¹⁶ (ii) by using structure-directing agents such as various organic solvents.¹⁷ Our strategy in this work introduces a more drastic modification to the link–link interaction: two *Im* links are coupled by the organic bridge of hydrazone, and this additional N-donor site warrants the usage of octahedral metal ions, such as Zn^{II} (which can adopt both tetrahedral and octahedral configurations), Mn^{II} , Cu^{II} , and Ni^{II} , other than tetrahedral ones.

The complexes can be readily prepared by reacting the BIm ligand with various metal nitrate salts under solvothermal conditions (see the Supporting Information (SI) for experimental details). Four gyroidal MOFs with the formulas of $Zn(BIm)$ (STU-1), $Mn(BIm)$ (STU-2), $Cu(BIm)$ (STU-3), and $Ni(BIm)$ (STU-4) were obtained and characterized (the guest molecules are highly disordered). X-ray crystal analyses reveal they are isomorphous and all crystallize in the cubic space group of $Ia\bar{3}d$, which has the most complex crystallographic symmetry (see SI for crystallographic details). The large-scale polycrystalline sample of STU-1 can be obtained with high yield by slow-diffusion method, identified by powder X-ray diffraction studies (Figure S5 in SI).

As an example, the structure of STU-1 will be described in detail, and compared with those of related ZIFs and zeolites. As shown in Figure 1a, the Zn^{II} center is five-coordinated and adopts a distorted square pyramidal geometry, fulfilled by four *Im*-N sites and one additional hydrazone-N. This coordination geometry is different from the commonly observed tetrahedral mode for Zn^{II} in ZIFs,¹⁶ and can be considered as a unsaturated octahedral metal sites (note in STU-4 the vacant octahedral Ni^{II} site is completed by a water molecule, see Figure S1c in SI). One notable detail is one *Zn*–*Im* bond is not coplanar with the *Im* ring (*Zn*–*N*–*N*–*Zn* dihedral angle 19.8° ; *Zn*–*Im*–*Zn* angles 132.79° and 149.10°), whereas in most ZIFs, the *M*–*Im* bonds are coplanar with the *Im* rings (e.g., in ZIF-20 *Zn*–*N*–*N*–*Zn* dihedral angles range from 0 to 0.15° ; *Zn*–*Im*–*Zn* angles close to 145°).^{13,16} This subtle difference creates a curvature that accounts for the formation of the typical helical-ribbon motif in the gyroid (vide infra). The overall framework of STU-1 can still be envisaged as constructed from tetrahedral Zn^{II} vertices (Figure 1b) because the additional hydrazone bridge, though links two *Im* groups and coordinates to the Zn^{II} site, has no topological significance to the extended structure. But the tetrahedral Zn^{II} vertices, with surrounding angles ranging from 98.38° to 140.33° , are highly distorted from the ideal tetrahedral nodes (109.48°) in zeolites.

Received: September 13, 2011

Published: November 07, 2011

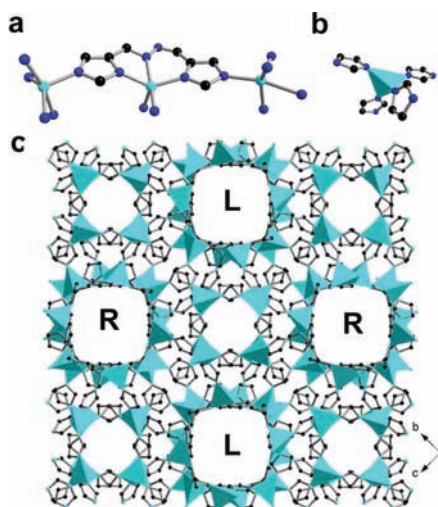


Figure 1. (a) Coordination geometry of Zn^{II} and Bim in STU-1 (color codes: Zn, cyan; N, blue; C, black; H, omitted). (b) The distorted tetrahedron of the Zn^{II} vertex fulfilled by four Im groups; the organic bridge ($-\text{C}=\text{N}-\text{N}=\text{C}-$) is omitted. (c) The overview of the 3D framework of STU-1 along the a -axis, showing the left-handed (L) and right-handed (R) helical channels therein.

Viewed from the a direction, there are alternatively arranging left-handed and right-handed helical channels (Figure 1c). These helical ribbons (pitch 34.647 Å, equal to unit cell length; width 6.2 Å) made up of edge-sharing 4-membered rings (Figure 2a,b) propagate along three cubic axial directions, and three of them with the same handedness intersect with each other to form a 12-ring window with the dimension of ca. $27.3 \text{ \AA} \times 15.4 \text{ \AA}$ (Figure 2c), which is another typical structural feature of the gyroid. There also exists another type of helical ribbon, with vertex-sharing 4-membered rings, running along the 111 direction (Figure S2 in SI). Three 12-ring windows encompass a unique helical pore (Figure 2d,e), which is connected to three adjacent cavities with the same handedness to form a gyroidal channel system. Interestingly, two independent sets of helical pores with opposite handedness are separated by the crystalline wall of STU-1 (Figure 2d). The large voids of STU-1 (21294.4 \AA^3 in one unit cell, 51.2%, checked by PLATON) are separated to two parts, as demonstrated by the SQUEEZE program in PLATON, showing two major equal squeeze-void-volumes of ca. 10010 \AA^3 for each. In fact, this is an intrinsic and the most remarkable feature of the gyroid: the whole space is divided into the right-handed and left-handed regions by a bicontinuous G minimal surface. The framework of STU-1 precisely lies on this surface; in other words, this “elusive yet ubiquitous”¹ mathematical model may underlie the formation of the high-symmetry MOFs in this work.

To gain a better visualization and understanding of the relation between STU-1 and the gyroid, the approach of nets and tilings¹² is considered. In a word, any space can be seamlessly embedded by (periodic or aperiodic) tiles; tiles carry nets; frameworks of extended structures (such as those of MOFs) can be topologically simplified into nets. By denoting the Zn^{II} vertices as distorted tetrahedral nodes, the framework of STU-1 (viewed down the 111 direction, Figure 3a) can be simplified as a uninoal three-periodic net (Figure 3b) with the point symbol of $4^3.6^3$ and vertex symbol of $4.4.4.6.12_{69}.12_{69}$, which is collected in RCSR¹⁸ as the **gie** net. The corresponding underlying $4^3.6$

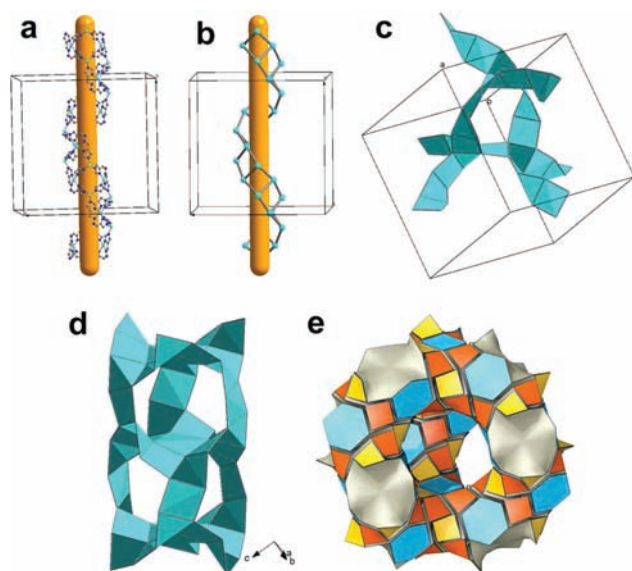


Figure 2. Partial views of the gyroidal features in STU-1. (a) Left-handed helical ribbon constructed from two Zn–Bim chains along the b -axis. (b) Topologically simplified helical ribbon showing the edge-sharing 4-membered rings (Zn vertices as cyan nodes). (c) Three helical ribbons (showed in cyan) along three cubic axes cross-linking to form a 12-ring window. (d) Two sets of helical pores (each with three 12-ring windows) with opposite handedness separated by the G surface. (e) Tiling representation of the helical pore with the tiles slightly shrunk and different faces (4 kinds) colored differently. Note that only half tiles are shown; the rest of the space would be filled by an identical set of tiles.

tiling (transitivity 1242, meaning with 1 kind of vertex, 2 kinds of edges, 4 kinds of faces, and 2 kinds of tiles, see Figure S4 in SI) is illustrated in Figure 3c. As mentioned, the G surface separates the space into two helical channel systems, and hence, only half of the tiles that complete one helical channel system are depicted; the G surface (and also the framework of STU-1) thus lies on the colored faces (orange, yellow, and blue ones) of the model. It is interesting to note that the gyroid can be realized by different topologies, such as the **fcy** and **fcz** nets and their different $3^2.4.3.6$ tilings,^{7,12} and also it can be defined as the space that separates two interpenetrated **srs** net¹ with the interpenetration class IIa (a detailed comparison of the reported **srs-c** and **gie** structures is given in the SI).¹⁹

A survey in the Cambridge Structural Database (CSD version 5.32, November 2010) targets only 38 crystal structures with $Ia\bar{3}d$ space group, 11 of which are coordination polymers. Among them, four reported (first by Chen et al.²⁰ and subsequently by Tian et al.²¹) ZIFs with **ana** topology, mimicking the ANA zeolite, also follow the gyroid as building prototype, but this has never been claimed. ANA is the only zeolite following the G surface until the discovery of the BSV zeolites (UCSB-7 series).⁶

STU-1 is to compare with BSV⁶ because of their similar forms and functions. They both have the **gie** topology with the underlying model of the gyroid, while STU-1 surpasses BSV in the following aspects. (i) STU-1 is symmetrically closer to the model of the gyroid: it crystallizes in a centric $Ia\bar{3}d$ space group, identical to the maximum symmetry of the gyroid, whereas BSV (UCSB-7K) exhibits a lower symmetry with a noncentric, chiral $I2_13$ space group. (ii) The unit cell volume of STU-1 ($41591.1(4) \text{ \AA}^3$) is much larger than that of BSV ($6514.69(6) \text{ \AA}^3$), while the density of metal atoms per unit volume of STU-1 (2.31 nm^{-3}) is

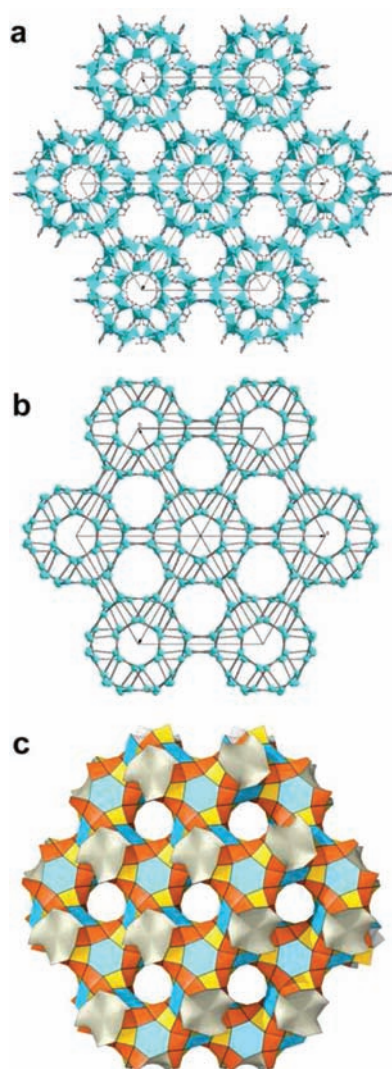


Figure 3. Representation of the gyroidal structure of STU-1 viewed down the 111 direction. (a) Framework representation showing the Zn^{II} vertices as cyan distorted tetrahedra. (b) Net representation by denoting the Zn^{II} ions as 4-connected nodes (shown in cyan) and the BIm ligands as linkers. (c) Tiling representation wherein only half tiles are shown, considering one helical channel system is filled by 2 kinds of tiles with 4 kinds of faces (colored differently).

much smaller than that of BSV (14.7 nm^{-3}). (iii) The thermal stability of STU-1 is exceptional: it can stay stable at high temperature up to $420 \text{ }^\circ\text{C}$ at N_2 atmosphere, revealed by thermal gravimetric analysis (Figures S7, S9, and S10 in SI), whereas the inorganic BSV zeolites are not stable in the range of $250\text{--}400 \text{ }^\circ\text{C}$. Moreover, under vacuum condition, STU-1 is found to maintain crystallinity at high up to $650 \text{ }^\circ\text{C}$, testified by variable-temperature powder X-ray diffraction (PXRD, Figure S8 in SI).

The chemical stability of STU-1 was also attested by suspending the crystal samples of STU-1 in boiling toluene and methanol– NaBH_4 for 24 h. IR spectra indicate that the hydrazone group is not reduced to amine by NaBH_4 even under boiling condition, and PXRD patterns (Figure S12 in SI) show that the solid samples sustain full crystallinity and local structure after the treatments. The exceptional thermal and chemical stabilities of STU-1 is comparable to those of the most stable porous ZIFs,²²

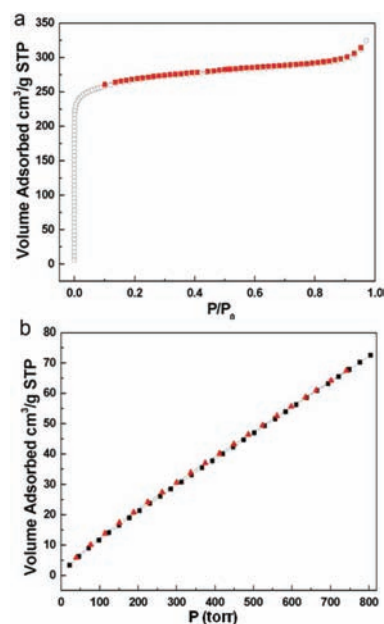


Figure 4. Gas adsorption isotherms of STU-1. (a) N_2 adsorption at 77 K ; open circles and filled red squares represent adsorption and desorption, respectively. (b) CO_2 adsorption at 273 K ; filled black squares and red triangles represent adsorption and desorption, respectively.

which is probably attributed to the additional covalent hydrazone bridge and its coordination to the Zn^{II} site.

Preliminary measurements of the sorption behavior were performed. The permanent porosity of STU-1 is confirmed by N_2 adsorption isotherm measurements (Figure 4a), exhibiting type I adsorption isotherm for typical microporous materials. The Langmuir and Brunauer–Emmett–Teller (BET) surface areas are calculated to be 1225 and $775 \text{ m}^2/\text{g}$, respectively. This BET surface area is considered moderate compared with those of reported ZIFs,¹⁶ but the CO_2 capture ability ($70.2 \text{ cm}^3/\text{g}$ or $138.7 \text{ g}/\text{kg}$ at 273 K , Figure 4b) of STU-1 is comparable to the best-performing ZIF for CO_2 reservoir, that is, ZIF-69 with the ability of $126.1 \text{ g}/\text{kg}$.^{14,16} We will investigate the metal-site-dependent adsorption behaviors and gas separation properties²³ of the gyroidal STU-1 to 4 in the near future.

The gyroid has found far-reaching applications in nanoporous carbon materials²⁴ and mesoporous silica materials²⁵ for gas storage. It is unclear whether the labyrinthine feature of the G surface also plays a part to some extent in the gas adsorption behavior of gyroidal MOFs, but clearly it deserves to be addressed further, preferably by molecular simulation, such as a recent work dealing with the effect of pore topology and accessibility on gas adsorption capacity of ZIFs.²⁶

We anticipate the gyroidal metal–organic frameworks with crystalline ordering at the atomic level to attract the attention of mathematicians whose expertise lies on differential geometry and minimal surfaces, and to serve as a promising plateau for the burgeoning applications of ZIFs, thus, closing the gap between the academic and industrial sectors.

■ ASSOCIATED CONTENT

S Supporting Information. Experimental details, X-ray crystallographic data, additional figures and descriptions, topological analysis details, and physical measurements (IR, TGA and

PXRD). This material is available free of charge via the Internet at <http://pubs.acs.org>.

AUTHOR INFORMATION

Corresponding Author

dli@stu.edu.cn

ACKNOWLEDGMENT

We thank Professor Michael O'Keeffe of Arizona State University for his helpful discussions on the structures and topology. This work is financially supported by the National Basic Research Program of China (973 Program, 2012CB821706), the National Natural Science Foundation for Distinguished Young Scholars of China (20825102), the National Natural Science Foundation of China (21171114, 21101103) and Shantou University.

REFERENCES

- (1) Hyde, S. T.; O'Keeffe, M.; Proserpio, D. M. *Angew. Chem., Int. Ed.* **2008**, *47*, 7996–8000.
- (2) Andersson, S.; Hyde, S. T.; Larsson, K.; Lidin, S. *Chem. Rev.* **1988**, *88*, 221–242.
- (3) Hyde, S. T.; Andersson, S.; Larsson, K.; Blum, Z.; Landh, T.; Lidin, S.; Ninham, B. W. *The Language of Shape*; Elsevier: Amsterdam, 1997.
- (4) Saranathan, V.; Osuji, C. O.; Mochrie, S. G. J.; Noh, H.; Narayanan, S.; Sandy, A.; Dufresne, E. R.; Prum, R. O. *Proc. Natl. Acad. Sci. U.S.A.* **2010**, *107*, 11676–11681.
- (5) Kresge, C. T.; Leonowicz, M. E.; Roth, W. J.; Vartuli, J. C.; Beck, J. S. *Nature* **1992**, *359*, 710–712.
- (6) Gier, T. E.; Bu, X.; Feng, P.; Stucky, G. D. *Nature* **1998**, *395*, 154–157.
- (7) Zou, X.; Conradsson, T.; Klingstedt, M.; Dadachov, M. S.; O'Keeffe, M. *Nature* **2005**, *437*, 716–719.
- (8) Armatas, G. S.; Kanatzidis, M. G. *Nature* **2006**, *441*, 1122–1125.
- (9) Sun, J.; Bonneau, C.; Cantin, A.; Corma, A.; Diaz-Cabanas, M. J.; Moliner, M.; Zhang, D.; Li, M.; Zou, X. *Nature* **2009**, *458*, 1154–1157.
- (10) Long, J. R.; Yaghi, O. M. *Chem. Soc. Rev.* **2009**, *38*, 1213–1214.
- (11) Chen, B.; Eddaoudi, M.; Hyde, S. T.; O'Keeffe, M.; Yaghi, O. M. *Science* **2001**, *291*, 1021–1023.
- (12) Delgado-Friedrichs, O.; Foster, M. D.; O'Keeffe, M.; Proserpio, D. M.; Treacy, M. M. J.; Yaghi, O. M. *J. Solid State Chem.* **2005**, *178*, 2533–2554.
- (13) Hayashi, H.; Côté, A. P.; Furukawa, H.; O'Keeffe, M.; Yaghi, O. M. *Nat. Mater.* **2007**, *6*, 501–506.
- (14) Banerjee, R.; Phan, A.; Wang, B.; Knobler, C.; Furukawa, H.; O'Keeffe, M.; Yaghi, O. M. *Science* **2008**, *319*, 939.
- (15) Wang, B.; Côté, A. P.; Furukawa, H.; O'Keeffe, M.; Yaghi, O. M. *Nature* **2008**, *453*, 207–211.
- (16) Phan, A.; Doonan, C. J.; Uribe-Romo, F. J.; Knobler, C. B.; O'Keeffe, M.; Yaghi, O. M. *Acc. Chem. Res.* **2010**, *43*, 58–67.
- (17) Tian, Y.-Q.; Zhao, Y.-M.; Chen, Z.-X.; Zhang, G.-N.; Weng, L.-H.; Zhao, D.-Y. *Chem.—Eur. J.* **2007**, *13*, 4146–4154.
- (18) O'Keeffe, M.; Peskov, M. A.; Ramsden, S. J.; Yaghi, O. M. *Acc. Chem. Res.* **2008**, *41*, 1782–1789.
- (19) Alexandrov, E. V.; Blatov, V. A.; Kochetkov, A. V.; Proserpio, D. M. *CrystEngComm* **2011**, *13*, 3947–3958.
- (20) Huang, X.-C.; Lin, Y.-Y.; Zhang, J.-P.; Chen, X.-M. *Angew. Chem., Int. Ed.* **2006**, *45*, 1557–1559.
- (21) Tian, Y.-Q.; Yao, S.-Y.; Gu, D.; Cui, K.-H.; Guo, D.-W.; Zhang, G.; Chen, Z.-X.; Zhao, D.-Y. *Chem.—Eur. J.* **2010**, *16*, 1137–1141.
- (22) Park, K. S.; Ni, Z.; Côté, A. P.; Choi, J. Y.; Huang, R.; Uribe-Romo, F. J.; Chae, H. K.; O'Keeffe, M.; Yaghi, O. M. *Proc. Natl. Acad. Sci. U.S.A.* **2006**, *103*, 10186–10191.
- (23) Britt, D.; Furukawa, H.; Wang, B.; Glover, T. G.; Yaghi, O. M. *Proc. Natl. Acad. Sci. U.S.A.* **2009**, *106*, 20637–20640.
- (24) Kowalczyk, P.; Hołyst, R.; Terrones, M.; Terrones, H. *Phys. Chem. Chem. Phys.* **2007**, *9*, 1786.
- (25) Han, L.; Miyasaka, K.; Terasaki, O.; Che, S. J. *Am. Chem. Soc.* **2011**, *133*, 11524–11533.
- (26) Babarao, R.; Dai, S.; Jiang, D.-e. *J. Phys. Chem. C* **2011**, *115*, 8126–8135.